Soft Matter

Cite this: *Soft Matter*, 2011, **7**, 6522

www.rsc.org/softmatter

PAPER

Self-assembled nanostructures of bottle-brush polyelectrolytes with oppositely charged surfactants: a computational simulation study†

Qianqian Cao,* Chuncheng Zuo, Lujuan Li and Hongwei He

Received 28th March 2011, Accepted 3rd May 2011
DOI: 10.1039/c1sm05528c

Recent experiments have revealed several morphologies of complexes formed by the self-assembly of bottle-brush polyelectrolytes (BPEs) and oppositely charged surfactants. We report herein a computational study of the formation and transition of self-assembled BPE/surfactant complexes with varying the backbone stiffness and amount of added surfactant. We characterize five complex shapes distinguished on the basis of BPE conformations and aggregate morphologies. Our simulations suggest that for cases of single adsorbed aggregate with an almost complete contact with the BPE, the backbone adopts a helical conformation regardless of the molecular details, while the helical fashion shows a dependence on the investigated parameters. Moreover, a spiral aggregate is observed at high backbone stiffness and BPE/surfactant charge ratio. The present results provide a valuable complement to experiment in exploring the possible structural phases of BPE/surfactant complexes at a molecular level.

1. Introduction

Highly ordered nanostructures, formed by the self-assembly of polyelectrolytes and oppositely charged surfactants, have attracted a great deal of scientific and industrial interest due to their intriguing structural diversity.[1–5] In solutions containing only surfactants, above the critical micelle concentration (cmc) they self-assemble into a wide variety of morphologically different structures ranging from micelles, vesicles, and bilayers to more complex mesophases such as crystal phases.[6–8] However, when the surfactants and polyelectrolytes are mixed in solution, the stable complexes exhibit well-defined supramolecular structures with different morphologies strongly depending on the charge ratio of surfactant to polyelectrolyte and the molecular architecture of polyelectrolyte chains. The high ordering of self-assembled complexes is driven by the cooperative binding fashion of surfactant molecules onto polyelectrolyte chains and the amphiphilicity of surfactant molecules. The non-covalent self-assembly strategy can easily control the sizes, shapes and functions of nanostructures by changing reaction and solvent conditions. Generally, the microphase separation in polyelectrolyte/surfactant complexes induced by the amphiphilicity of surfactants tends to lead to the formation of periodic nanostructures.

Most of the previous works on the self-assembly of charged polymers and surfactants have been focused on linear polyelectrolytes.[2,5,9] However, there are relatively few works carried out on branched and dendronized polymers.[10–15] In recent years, significant advances in synthetic polymer chemistry have provided routes to prepare macromolecules with more sophisticated architecture and well-defined topology. Among various synthetic species, bottle-brush polyelectrolytes (BPEs) have received considerable attention from many research communities.[16,17] BPEs consist of a long backbone onto which polyelectrolyte chains are densely grafted. In the mixed solution of BPEs and oppositely charged surfactants, several experiments have reported that the structural transition of self-assembled complexes can be achieved by varying BPE/surfactant molar ratio, surfactant length, salt surfactant and pH.[18–20] Interestingly, the complexation of BPEs with surfactants was found to induce the formation of a hierarchical helical structure under appropriate conditions.[19] Moreover, in the presence of multivalent counterions, BPEs undergo an intermediate state in which the backbone adopts a helical conformation.[21] In these studies, BPEs share one common structural feature: they collapse to a compact state at high surfactant or multivalent counterion concentrations.

Our group is interested in exploring the formation and structural transition of complexes of oppositely charged surfactants with BPEs. Additionally, we also pay particular attention to the helical formation in self-assembled complex structures through noncovalent bonding interactions. Experimentally, amphiphilic block copolymers can self-assemble into a variety of supramolecular nanostructures including worm micelles, spherical micelles, multicompartment micelles, vesicles, toroids and

College of Mechanical Science and Engineering, Jilin University, Changchun, P. R. China 130022. E-mail: qqcao07@mails.jlu.edu.cn; Fax: +86-431-85095288; Tel: +86-431-85095288

† Electronic supplementary information (ESI) available: Initial configuration of the simulated system and some additional simulation results. See DOI: 10.1039/c1sm05528c

helices.[22–24] Recent reports indicated that the self-assembly of triblock copolymers form different helical structures such as single, double and triple helices.[25,26] Zhong *et al.* suggested that the driving force for helix formation from a supramolecular cylinder is a combination effect of long-range electrostatic interactions and uniaxial compression of the same cylinder.[26] Another interesting phenomenon is that the interaction of guest molecules with carbon nanotubes results in a self-assembled superstructure in which guest molecules helically wrap the nanotube surface. Examples include spiral wrapping of carbon nanotubes by DNA,[27] amphiphilic linear polymers[28] and surfactants.[29] For surfactant/nanotube composites, surfactant molecules develop into a helical micelle in the inner surface of hydrophilic nanotube. However, there are many other examples of helical structures driven by very different mechanisms of inter or intramolecular interactions, such as the intermolecular assembly of chiral molecules,[30,31] mechanical force[32,33] and entropy-driven helix formation.[34] To obtain a detailed description of synthesis and structural characteristics of helical macromolecules, we refer the readers to a recent review.[35] For BPE/surfactant complexes at an intermediate surfactant/PBE molar ratio, Schmidt and co-workers indicated that the helical conformation of the backbone is due to the hydrophobicity of the β-sheets formed by the side chain-surfactant complexes.[18] Though high molar ratio leads to the collapse state of BPEs, the structural details of the backbone at the molecular level have not been addressed so far.

Concern about the complex formation of BPEs with oppositely charged surfactants is a recent development. To our limited knowledge, only two groups of Müller and co-workers[20] and Schmidt and co-workers[18,19] have performed original experimental studies as mentioned above. Nevertheless, a thorough understanding of the morphological transition between various assemblies as well as the relation between self-aggregation and molecular structure is still lacking. Moreover, it is very difficult to carry out a series of experiments over a wide range of parameters in order to find all possible complex structures. In this work, we carry out Brownian dynamics (BD) simulations using a coarse-grained bead-spring model to reveal the possible nanostructures formed by a BPE and surfactants as well as their transitions when varying the backbone stiffness and the surfactant concentration. Additionally, we do not take into account the chemical details of molecular chains to study the general structural characteristics of BPE/surfactant complexes. The coarse-grained bead-spring model has been extensively applied in computational modelling of synthetic polymers and biomacromolecules, such as self-assembly of surfactant molecules.[36–39]

2. Model and simulation method

We employed a coarse-grained model to represent both the BPE and oppositely charged surfactants. The BPE consists of one neutral backbone with $N_m = 100$ monomers and $N_c = 50$ negatively charged side chains. Each side chain includes $N_{cm} = 9$ charged monomers. Every second of the backbone monomers carries one side chain. We represent the surfactant with one positively charged head group and $N_{sm} - 1$ hydrophobic tail beads. If not otherwise stated, the surfactant length is taken as $N_{sm} = 9$. The number of surfactant molecules, N_s, is chosen as a variable parameter to study the effect of the surfactant concentration c_s on the structure of the surfactant/BPE complex. In order to neutralize the solution, $N_c N_{cm}$ cations and N_s anions are added into the system. All particles are enclosed in a cubic simulation box with a box length $L = 140\sigma$ (Supporting Information, Figure S1†), and periodic boundary conditions are applied in all three directions. Our simulation box is large enough to avoid short-range interactions of the BPE with its periodic images. The range of surfactant concentrations investigated is between $c_s = 0$ and $3.3 \times 10^{-4}\sigma^{-3}$ (corresponding to N_s from 0 to 900). If solvent particles are explicitly included in the system with a typical number density of $\rho = 0.8\sigma^{-3}$, it creates a large system with about 2.2×10^6 particles. To obtain equilibrium properties of the complex, it is almost impossible to simulate such system consisting of so many particles due to limitations in the required computer power. However, the implicit solvent model only contains 1×10^4 particles for the highest surfactant concentration studied.

The model potentials used in the paper have been described in our recent works.[40] Here, we only give the necessary details on the potential parameters. The short-range interaction between any two particles is modeled by the truncated-shifted Lennard–Jones (LJ) potential. We take σ, m and ε_{LJ} (for the BPE–BPE interaction) as length, mass and energy units, respectively. All other units are derived from these basic units, such as time unit $\tau = (m\sigma^2/\varepsilon_{LJ})^{1/2}$ and temperature unit $T^* = \varepsilon_{LJ}/k_B$ (k_B is the Boltzmann constant). For all particle pairs except the tail–tail ones, the cutoff distance is taken to be $r_c = 2^{1/6}\sigma$. To model the hydrophobic surfactant tail, we introduce an attractive cutoff $r_c = 2.5\sigma$ for the tail–tail interaction. The LJ potential strength between tail beads is set to $\varepsilon_{LJ} = 1.5k_BT$ corresponding to a relatively strong hydrophobic interaction, while $\varepsilon_{LJ} = 1.0k_BT$ is chosen for other particle pairs. The chain's connectivity is maintained by a finitely extendable nonlinear elastic (FENE) potential.[41] We take into account the bending rigidity of the backbone through using a harmonic angle potential. A fully flexible backbone is mimicked by setting $k_\theta^* = 0$, and $k_\theta^* = 450$ corresponds to a strong chain stiffness where k_θ^* is the dimensionless stiffness $k_\theta^* = k_\theta rad^2/\varepsilon_{LJ}$. An intermediate range of the stiffness constant, $10 \leq k_\theta^* \leq 300$, is also included to model the semiflexible backbone. Additionally, to investigate the case of a completely rigid backbone, the backbone monomers are frozen and evenly arranged in a straight line. Neighboring monomers in the backbone are separated by an equilibrium bond length of $l_b = 0.98\sigma$. Electrostatic interactions are calculated using the particle–particle/particle-mesh (PPPM) algorithm.[42] A temperature of $T = 1.2T^*$ is maintained by a Langevin thermostat.[43] The positions and velocities of the particles are solved using the velocity-Verlet algorithm with a time step $\Delta t = 0.008\tau$. Initially, surfactants are randomly dispersed within the simulation box. The time which the system reaches the equilibrium state depends on surfactant concentration, backbone stiffness and initial distribution of the surfactants. After achieving a steady state, a production run of 2.5×10^6 time steps is performed to obtain some equilibrium properties. In this work, we choose $\sigma = \lambda_B$ where $\lambda_B = e^2/(4\pi\varepsilon_0\varepsilon_r k_B T)$ is the Bjerrum length, ε_0 and ε_r are the vacuum permittivity and the dielectric constant of the solvent, respectively. The Bjerrum length for water is 0.71 nm at room

temperature. Therefore, the largest surfactant concentration studied here is $c_s = 1.5 \times 10^{-3}$ mol L^{-1}.

3. Results and discussion

3.1 Self-assembly process

It is expected that the change of backbone stiffness can influence the morphology of the surfactant aggregates adsorbed on the BPE. We first study two cases: the BPE with a strong rigid backbone of $k_\theta^* = 450$ and that with a fully flexible backbone. In the following discussion, we use the dimensionless charge ratio $\beta = N_s/N_cN_{cm}$ instead of the surfactant concentration c_s to characterize the relation between the charge amount of surfactants and that of the BPE, because the number of adsorbed surfactants seems to have a direct dependence on β. In order to gain quantitative information on the formation process of BPE/surfactant complexes, Fig. 1 shows the time evolutions of the number M_{max} of surfactants in the largest aggregate electrostatically adsorbed to the BPE and the total adsorption amount M_{tot}. Unless otherwise stated, aggregates refer to those adsorbed to the BPE, as opposed to free aggregates in solution. A rapid increase in the adsorption amount is observed at the initial simulation stage. This is due to the fact that the surfactants initially exist in single molecules or small aggregates, resulting in relatively strong diffusion ability. Meanwhile, the high negative charge in the complex induces a strong attraction force and thus facilitates the movement of surfactants towards the BPE. After a long simulation time, the maximum aggregate size is still inconsistent with the adsorption amount at a small amount of added surfactants (*i.e.*, $\beta = 0.6$ for $k_\theta^* = 450$ and $\beta = 0.4$ for completely flexible backbone), meaning that different aggregates can not merge into a single larger micelle. At $\beta = 1.0$, the formation of multiple aggregates only occurs during a relatively short time ($t < 1.1 \times 10^4\tau$) for the case of flexible backbone (Fig. 1b). However, at $k_\theta^* = 450$, the aggregate merging takes very long time ($t < 6.1 \times 10^4\tau$) to achieve a stable single aggregate (Fig. 1a).

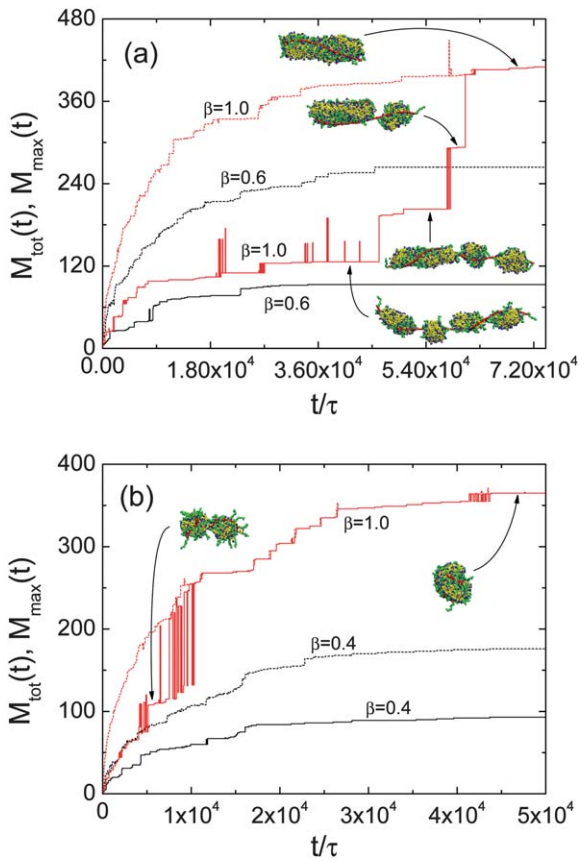

Fig. 1 Time evolution of the number M_{max} (solid line) of surfactants in the largest adsorbed aggregate and the total number M_{tot} (dashed line) of adsorbed surfactants on the BPE. (a) and (b) correspond to the case of the backbone stiffness $k_\theta^* = 450$ and that of fully flexible backbone, respectively. Color scheme: head particles of surfactant (blue), tail particles of surfactant (yellow), backbone particles (red) and side chain particles (green). Counterions and non-adsorbed surfactants are not shown for clarity.

As seen from Fig. 1a, the size of the largest aggregate often increases by a value less than 20, but it occasionally becomes larger by a higher value, *i.e.*, 71, 92 and 107 corresponding to three different merging stages. It is clear that the slow increase is due to the adsorbed aggregates by addition of single surfactants or free micelles. Note that the vertical bands represent the fluctuation of the aggregates approaching each other within a very small range. The initial binding of surfactants with the BPE occurs at multiple different sites. The flexible backbone quickly collapses to a coil state due to its random fluctuation inducing a fast aggregate fusion, while for the backbone with high stiffness, the incorporation of neighboring surfactant aggregates mainly depend on the local bending of the backbone and the deformation of adsorbed micelles through interactions between them and side chains. More precisely, the bending of the backbone is caused by the resistance of aggregates to the change of their preferred shape, while conversely the difficulty in bending the backbone drives the reshaping of aggregates. It is worth emphasizing that the electrostatic attraction between side chains and oppositely charged surfactant heads plays a critical role in bridging those two kinds of deformation mechanisms. In Fig. 1a, the results at $\beta = 1.0$ indicate that there is a slow increase in the adsorption amount after a long simulation time ($t < 4.5 \times 10^4\tau$), whereas adjacent aggregates are just beginning to merge together. Therefore, enhancing the backbone stiffness lowers the merging rate. Additionally, we also give several typical snapshots at different charge ratio (Supporting Information, Figure S2–S3†).

We want to point out that when the adsorption amount reaches an equilibrium value, the structure of the complex is not necessarily in a final stable state. Therefore, a sufficiently long simulation is performed after the adsorption amount remains constant. We monitor the morphology change of the complex at different simulation stages. The final structure is determined until the morphology of the complex is in a stable state. At the lowest charge ratio studied, $\beta = 0.2$, it takes a relatively short time to obtain the stable structure of the complex. At high charge ratios and strong backbone stiffness, the complex exhibits a stable structure after a longer time due to a local morphology adjustment.

3.2 Adsorption behavior of surfactants on the BPE

In the above discussion, we give a general description of the self-assembled structures when the BPE backbone is fully flexible or

highly rigid. We now continue to perform a study on the adsorption properties of surfactants under a different charge ratio and variable backbone stiffness. It is found that the adsorption amount increases linearly with the charge ratio at $\beta < 0.8$ and does not depend on the chain stiffness (Fig. 2). This result suggests that almost all surfactant molecules are bound to the BPE because of strong diffusion ability and a high charge of the complex with the opposite sign to that of the surfactant as discussed above. The strong diffusion is ascribed to the fact that low surfactant concentration makes it difficult to form large free aggregates in the adsorption time. At a high charge ratio, a distinct difference in adsorption amount reveals that the chain stiffness significantly influences the number of adsorbed surfactants by tuning the aggregate shape. For example, at $\beta = 2.0$, the adsorption fraction for fully flexible case is 52% ($M_{tot} = 470$), while 59% ($M_{tot} = 535$) at $k_\theta^* = 450$. Additionally, we do not rule out the effect of random thermal fluctuation. We have monitored the evolution of the largest free micelles. All simulations show that the surfactant number included in such micelles does not exceed 20. Unlike those free micelles, the formation of larger micelles located at the BPE is driven by a cooperative binding fashion, that is, the interaction between neighboring surfactant molecules facilitates to develop a larger aggregate in the vicinity of previously adsorbed surfactants. A similar conclusion is drawn for brush/surfactant systems.[44] However, the structural characteristics of surfactant aggregates have been less addressed systematically.

If the amount of adsorbed surfactants is higher than that required to neutralize the BPE (namely, $M_{tot} > N_c N_{cm}$), the BPE is overcharged by oppositely charged surfactants, also known as charge inversion. As shown in Fig. 2, the system is found in an overcharged state at a high charge ratio of $\beta = 2.0$. The overcharging phenomenon often occurs when a linear polyelectrolyte chain[45] or DNA[46] wraps around an oppositely charged object. However, there does not exist a common statement to explain the mechanism of charge inversion observed in different applications and the origin of overcharging is not clearly established for some cases. In the present study, it seems to be clear that the overcharging of the BPE at $\beta = 2.0$ is mainly related to the cooperative binding manner inducing the formation of larger aggregates. The increase in the adsorption amount

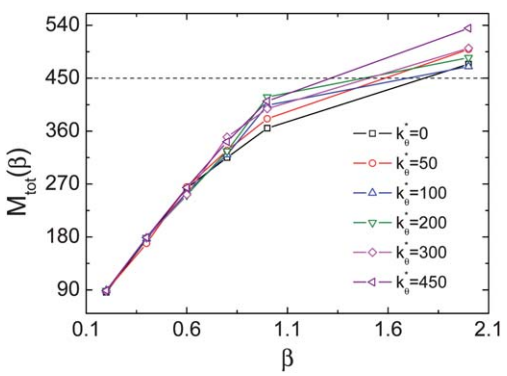

Fig. 2 Total number M_{tot} (dashed line) of adsorbed surfactants as a function of the charge ratio β at different backbone stiffness. Computational data are obtained after BPE/surfactant complexes reach a stable state.

also reduces the opportunity of approaching of free surfactants or small micelles to the BPE due to an enhanced long-range electrostatic repulsion. Experiments on planar[44,47,48] and spherical polymer brushes[49] indicated that the adsorption ratio of M_{tot} to $N_c N_{cm}$ depends on many factors, such as grafting density, hydrophobicity of grafted chains, surfactant concentration and surfactant length. In an intermediate range of surfactant concentrations, it was found that the rate of adsorption increase in a hydrophilic NaPSS was suppressed due to a balance of aggregation formation and excluded volume repulsion.[48] In the present work, the surfactant molecules at high surfactant concentrations are not completely adsorbed on the BPE to form a larger complex, especially for $\beta = 2.0$ (the adsorption fraction decreases significantly though there is an increase in the adsorption amount). Similarly, we believe that this behavior is due to a competition of aggregation formation and electrostatic attraction between surfactants and polyelectrolytes. Unlike planar polyelectrolyte brushes usually fixed on solid surfaces, spherical polyelectrolyte brushes coated on the surface of nanoparticles or colloid particles suspend in solution and diffuse freely, similar to the BPEs (though there is a different grafting manner). Note that almost all of surfactant molecules at $\beta \leq 1.0$ are taken up by spherical polyelectrolyte brushes.[49] The BPE/surfactant system also shows a high adsorption fraction between 0.82 and 0.93 at $\beta = 1.0$ depending on the backbone stiffness, above 0.9 at $\beta < 1.0$.

In order to quantitatively study the size of the BPE, we measure its root-mean-square radius of gyration R_g as a function of β under different backbone stiffness (Supporting Information, Figure S4a†). A significant decrease of R_g is observed at $\beta < 0.8$ in the range of chain stiffness investigated. However, with further increasing the surfactant amount, a remarkable reswelling behavior of the BPE only takes place at $k_\theta^* = 450$.

3.3 Phase behavior of BPE/surfactant complexes

To get an overview of the structural transition of BPE/surfactant complexes in the parameter regimes studied, we attempt to depict the complex structures in a phase plot using the parameters β and k_θ. Remember that the transitional boundaries of phase structures are not accurately described. Here, we aim to explore the possible stable structures through providing a phase diagram. All structures obtained from our numerical simulations can be divided into two main categories according to the number of aggregates adsorbed to the BPE: multiple aggregates and a single one. For the former, we also include a structure with one aggregate but only a small part of the backbone wrapped around this aggregate. Structures falling into the latter category are classified into four subgroups. Finally, we present five different structural phases P1–P5 of BPE/surfactant complexes as shown in Fig. 3. From an aggregate-centered viewpoint, the phases of BPE/surfactant complexes including one aggregate, P2–P5, correspond to an irregular aggregate, straight short rod, twisted slab and helix cylinder, respectively. Some typical snapshots marked with dashed lines mean that the aggregate may evolve into an irregular state when changing the initial configuration.

Undoubtedly, the structure P1 tends to occur at low surfactant concentrations and high backbone stiffness. Moreover, small aggregates induce a mild local bending of the backbone with an

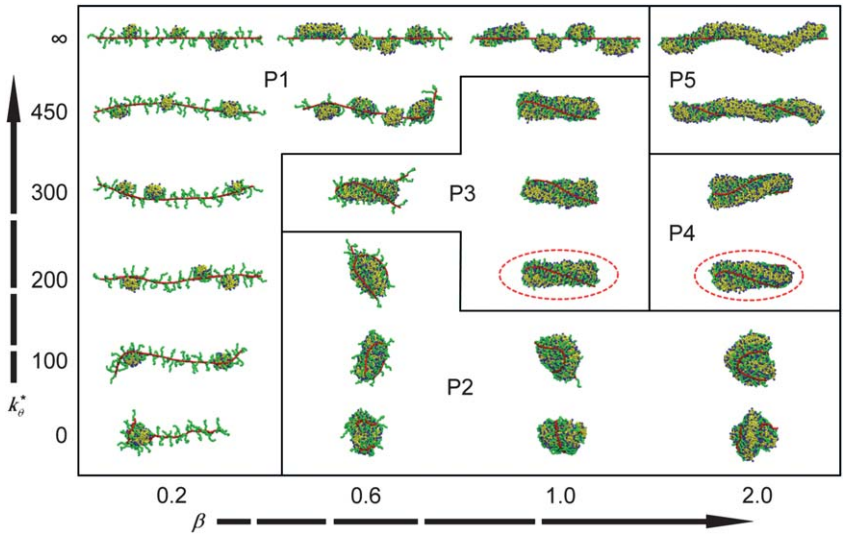

Fig. 3 Structural phase diagram of BPE/surfactant complexes with different self-assembled structures, plotted using parameters β and k_θ^*. The boundary lines are guides to the eye delineating the crossover regions between the different states. Counterions and non-adsorbed surfactants are not shown for clarity. The color scheme is the same as that used in Fig. 1. We display five different phases marked as P1–P5. The pictures are typical simulation snapshots of stable BPE/surfactant complexes.

extended conformation on the whole. When β exceeds a certain critical value, the adsorbed surfactants develop into a condensed structure P2 with irregular shape at relatively small values of k_θ^* and the backbone also collapses to a coiled state. Recent experiments show that the BPE/surfactant complexes are turned into compact globule at high β, and the molecular structure of BPE has a significant effect on the critical value of β at which the structural transition occurs.[19,20] At intermediate surfactant concentrations, increasing the backbone stiffness leads to a rod structure P3 and the backbone undergoes a backfolding process. Interestingly, in recent experiments, charged dendronized polymers form self-folded duplex supramolecular structures driven by preferred non-bonded interactions of the dendritic side chains with the polar solvent, and the self-folded morphology is also predicted by numerical simulations.[50] Moreover, the stable duplexes depend on a balance between non-bonded interactions and bending energy of the backbone. Though there exists differences in the formation mechanism of backfolding of the backbone for the BPEs and charged dendronized polymers, a common point is that the non-bonded interactions play an important role in triggering the assembly process. It is found that the structure P3 at a high charge ratio $\beta = 2.0$ transforms into two different states depending on the backbone stiffness. For example, in the case of a strong backbone stiffness $k_\theta^* = 450$, the backbone forms an extended helix at $\beta = 2.0$ meaning that further addition of the surfactant results in a release of the elastic restoring energy of the backbone (see Supporting Information, Figure S4b†). In contrast, under conditions of relatively weak stiffness, $k_\theta^* = 200$ and 300, the increase of β does not drive a significant change of the backbone conformation, but the aggregate adopts a structure very similar to a twisted slab (Fig. 4). Instinctively, some changes in the morphology of the complex induced by the backbone stiffness (such as conformational transition of the backbone from coiled to extended states) can be understood in terms of a simple argument that the bending force of the backbone balances the internal interactions in the aggregates originating from the hydrophobicity of the surfactant tails. However, this is unable to account for some details on the deformation of aggregates and the structural characteristics of the backbone.

One can note that for the structures P2–P5 (not including the case of completely rigid backbone), the backbone wraps around the aggregate to form a helix structure, while the charge ratio and the backbone stiffness primarily affect the helix state. The helix structure of the backbone was also observed in experimental studies on BPE complexes with oppositely charged surfactants,[18,19] trivalent ions[21] and linear polyelectrolytes.[51] In Fig. 5, we present several typical snapshots of BPE/surfactant complexes and BPEs with varying the backbone stiffness at a fixed charge ratio $\beta = 1.0$. Both cases of fully flexible and highly rigid backbone are given in Figure S2c–d and S3c–d (Supporting Information), respectively.† Apparently, a right-handed (Fig. 5b and Supporting Information Figure S2d†) or left-handed (Fig. 5c

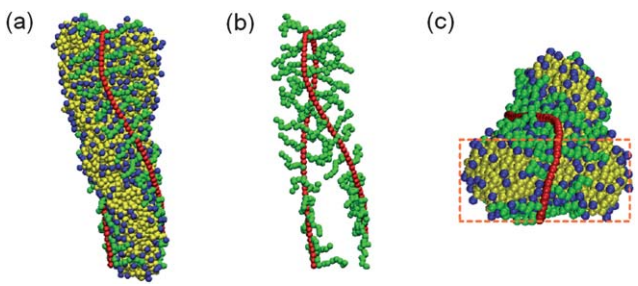

Fig. 4 (a) Twisted slab structure of the BPE/surfactant complex with a backbone stiffness $k_\theta^* = 300$ at $\beta = 2.0$. (b) To clearly observe the BPE structure, surfactant molecules are omitted. (c) The top view revealing a slab state of the surfactant aggregate is also shown. Counterions and non-adsorbed surfactants are not shown for clarity. The color scheme is the same as that in Fig. 1.

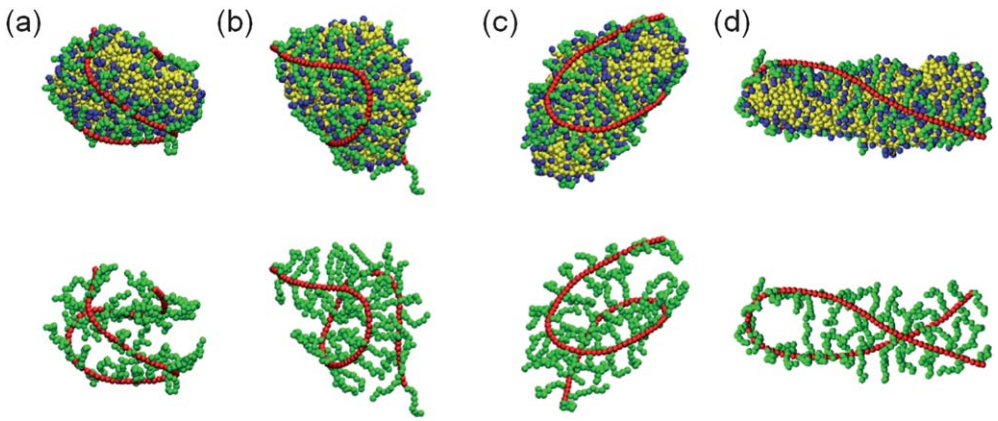

Fig. 5 Typical snapshots of the BPE/surfactant complex (upper panel) and the BPE without surfactants (lower panel) at $\beta = 1.0$, shown for four different helix states of the backbone (a)–(b). Counterions and non-adsorbed surfactants are not shown for clarity. The color scheme is the same as that used in Fig. 1. (a)–(d) correspond to the backbone stiffness (a) $k_\theta^* = 50$, (b) 100, (c) 150 and (d) 300.

and Supporting Information Figure S3d†) helix state of the backbone can be observed. This coexistence of handedness is reasonable since molecules used in the present simulations do not have specific chirality. Evidence for BPE/surfactant complexes of different handedness has been given experimentally.[18] The double-helix-like structure is another spiral pattern of the backbone as shown in Fig. 5d and S2c (Supporting Information).† A self-folded double-helix structure of the backbone for charged dendronized polymers was also observed.[50] Nevertheless, under some parameter conditions, we can not readily distinguish the helix form of the backbone (see Fig. 5a). Additionally, Figure S3c in Supporting Information shows that the backbone with a single-helix structure may wrap around the aggregate along two different winding directions.† Hopefully, one can obtain a clearer picture of the helix backbone or higher level structures by increasing the backbone length. Surprisingly, it is found that though the backbone is in a fully rigid state, the aggregate exhibits a helical morphology at $\beta = 2.0$ (see the regime P5 in Fig. 3). Note that the structure P5 at $k_\theta^* = 450$ is very similar to a complex structure in which a polymer or DNA helically winds a rigid carbon nanotube.[28] We believe that there should exist some relationship between the helical state of the backbone and that of the aggregate.

Now it is tempting to ask which mechanism controls the formation of the helix structure. A noticeable argument on helical self-assembly of triblock copolymers with di- or triethylenetetramine is that helix formation from a supramolecular cylinder is driven by long-range electrostatic interactions combined with uniaxial compression of the same cylinder.[26] Similarly, we speculate that most probably the origin of the helix morphology is established according to the contraction of the BPE along the backbone caused by the tendency towards the spontaneous state of aggregate. More importantly, this understanding has been supported by the contraction-induced helix formation of the BPE backbone in the presence of trivalent ions.[21] Halperin *et al.* have also suggested a mechanism in which the surfactant-induced contraction of the brush induces curvature.[52] It is worth noting that a different mechanism of helix formation of the backbones has been proposed by Schmidt and co-workers.[18] They suggested that the helix formation of the BPEs is driven by the hydrophobicity of the β-sheets formed by the side chain/surfactant complexes. Clearly, the differences in the mechanism of helix formation are due to different molecular structural characteristics such as side chain and surfactant length, aggregate size and chain hydrophobicity. Additionally, to gain insight into the effect of surfactant length on the complex structures, we present some additional results in Figure S5 and S6 of Supporting Information.†

4. Conclusions

In summary, we have studied the formation of nanostructures through the self-assembly of a bottle-brush polyelectrolyte (BPE) and oppositely charged surfactants using coarse-grained, Brownian dynamics (BD) simulations. Though the coarse-grained model simulations provide only qualitative information and are not quantitatively comparable with the experimental results, the simulation results obtained are sufficiently suggestive. Larin *et al.* have performed experimental investigations on the electrostatically-driven association of BPEs with oppositely charged linear polyelectrolytes, and used BD simulations, in which a similar coarse-grained model is employed, to probe the structural organization of BPE/polyelectrolyte complexes.[53] It is worth pointing out that in their investigations, the simulation results can predict the structural behavior of the assembled complexes obtained from the experiments. We also hope that the coarse-grained model can explore the general characteristics of the self-assembled complex at molecular level despite the loss of atomic details. Though the effect of the backbone stiffness on the structures of BPE/surfactant complexes have not been addressed experimentally, some results obtained here are supported by some related experiments.

In the range of parameters investigated, five different morphologies of BPE/surfactant complexes are identified by tuning the BPE/surfactant charge ratio and the backbone stiffness. One notable feature of the BPE/surfactant complex is the formation of helical shape of the backbone due to the surfactant-induced contraction of the BPE. Moreover, favorable helical patterns also show a considerable dependence on the charge ratio

and the backbone stiffness. Interestingly, at high backbone stiffness and charge ratio, the aggregate adopts a helical morphology. Hopefully, our work will offer some knowledge valuable for understanding the self-assembly process and structural transition of the BPE/surfactant complex. Manipulating the shape of surfactant aggregates by changing the structural parameters of BPEs may provide a strategy to obtain different morphological nanostructures. Finally, further work should be performed to obtain an experimental verification of the structures obtained in our study.

Acknowledgements

This work was supported by the National Natural Science Foundation of China under Grant 30770501.

References

1 M. Antonietti and A. Thünemann, *Curr. Opin. Colloid Interface Sci.*, 1996, **1**, 667–671.
2 S. Q. Zhou and B. Chu, *Adv. Mater.*, 2000, **12**, 545–556.
3 A. F. Thünemann, M. Müller, H. Dautzenberg, J.-F. Joanny and H. Löwne, *Adv. Polym. Sci.*, 2004, **166**, 113–171.
4 A. Perico and A. Ciferri, *Chem.–Eur. J.*, 2009, **15**, 6312–6320.
5 C. K. Ober and G. Wegner, *Adv. Mater.*, 1997, **9**, 17–31.
6 R. G. Laughlin, *The Aqueous Phase Behavior of Surfactants*, Academic Press, San Diego, 1994.
7 K. Holmberg, B. Jönsson, B. Kronberg and B. Lindman, *Surfactants and Polymers in Aqueous Solution*, 2nd ed., Wiley, Chichester, 2003.
8 S. Svenson, *Curr. Opin. Colloid Interface Sci.*, 2004, **9**, 201–212.
9 T. Nylander, Y. Samoshina and B. Lindman, *Adv. Colloid Interface Sci.*, 2006, **123**, 105–123.
10 G. Caminati, N. J. Turro and D. A. Tomalia, *J. Am. Chem. Soc.*, 1990, **112**, 8515–8522.
11 Y. Li, S. M. Ghoreishi, J. Warr, D. M. Bloor, J. F. Holzwarth and E. Wyn-Jones, *Langmuir*, 2000, **16**, 3093–3100.
12 R. Mészáros, L. Thompson, M. Bos, I. Varga and T. Gilányi, *Langmuir*, 2003, **19**, 609–615.
13 S. Q. Zhou, C. Burger and B. Chu, *J. Phys. Chem. B*, 2004, **108**, 10819–10824.
14 N. Canilho, E. Kasemi, A. D. Schluter, J. Ruokolainen and R. Mezzenga, *Macromolecules*, 2007, **40**, 7609–7616.
15 A. Mezei and R. Mészáros, *Soft Matter*, 2008, **4**, 586–592.
16 S. S. Sheiko, B. S. Sumerlin and K. Matyjaszewski, *Prog. Polym. Sci.*, 2008, **33**, 759–785.
17 N. Hadjichristidis, M. Pitsikalis, H. Iatrou and S. Pispas, *Macromol. Rapid Commun.*, 2003, **24**, 979–1013.
18 N. Gunari, Y. Cong, B. Zhang, K. Fischer, A. Janshoff and M. Schmidt, *Macromol. Rapid Commun.*, 2008, **29**, 821–825.
19 Y. Cong, N. Gunari, B. Zhang, A. Janshoff and M. Schmidt, *Langmuir*, 2009, **25**, 6392–6397.
20 Y. Y. Xu, S. Bolisetty, M. Ballauff and A. H. E. Müller, *J. Am. Chem. Soc.*, 2009, **131**, 1640–1641.
21 Y. Y. Xu, S. Bolisetty, M. Drechsler, B. Fang, J. Y. Yuan, L. Harnau, M. Ballauff and A. H. E. Müller, *Soft Matter*, 2009, **5**, 379–384.
22 D. J. Pochan, Z. Y. Chen, H. G. Cui, K. Hales, K. Qi and K. L. Wooley, *Science*, 2004, **306**, 94–97.
23 Z. B. Li, E. Kesselman, Y. Talmon, M. A. Hillmyer and T. P. Lodge, *Science*, 2004, **306**, 98–101.
24 X. S. Wang, G. Guerin, H. Wang, Y. S. Wang, I. Manners and M. A. Winnik, *Science*, 2007, **317**, 644–647.
25 J. Dupont, G. J. Liu, K. Niihara, R. Kimoto and H. Jinnai, *Angew. Chem., Int. Ed.*, 2009, **48**, 6144–6147.
26 S. Zhong, H. G. Cui, Z. Y. Chen, K. L. Wooley and D. J. Pochan, *Soft Matter*, 2008, **4**, 90–93.
27 B. Gigliotti, B. Sakizzie, D. S. Bethune, R. M. Shelby and J. N. Cha, *Nano Lett.*, 2006, **6**, 159–164.
28 Y. K. Kang, O. S. Lee, P. Deria, S. H. Kim, T. H. Park, D. A. Bonnell, J. G. Saven and M. J. Therien, *Nano Lett.*, 2009, **9**, 1414–1418.
29 N. Arai, K. Yasuoka and X. C. Zeng, *J. Am. Chem. Soc.*, 2008, **130**, 7916–7920.
30 A. Aggeli, I. A. Nyrkova, M. Bell, R. Harding, L. Carrick, T. C. B. McLeish, A. N. Semenov and N. Boden, *Proc. Natl. Acad. Sci. U. S. A.*, 2001, **98**, 11857–11862.
31 J. J. L. M. Cornelissen, M. Fischer, N. A. J. M. Sommerdijk and R. J. M. Nolte, *Science*, 1998, **280**, 1427–1430.
32 M. J. Buehler, Y. Kong and H. J. Gao, *J. Eng. Mater. Technol.*, 2004, **126**, 245–249.
33 J. R. Gladden, N. Z. Handzy, A. Belmonte and E. Villermaux, *Phys. Rev. Lett.*, 2005, **94**, 035503.
34 Y. Snir and R. D. Kamien, *Science*, 2005, **307**, 1067–1067.
35 E. Yashima, K. Maeda, H. Iida, Y. Furusho and K. Nagai, *Chem. Rev.*, 2009, **109**, 6102–6211.
36 L. Lenoci and P. J. Camp, *J. Am. Chem. Soc.*, 2006, **128**, 10111–10117.
37 G. K. Bourov and A. Bhattacharya, *J. Chem. Phys.*, 2003, **119**, 9219–9225.
38 S. J. Marrink, A. H. de Vries and A. E. Mark, *J. Phys. Chem. B*, 2004, **108**, 750–760.
39 G. Srinivas, S. O. Nielsen, P. B. Moore and M. L. Klein, *J. Am. Chem. Soc.*, 2006, **128**, 848–853.
40 Q. Q. Cao, C. C. Zuo, L. J. Li and N. Zhang, *Macromol. Theory Simul.*, 2010, **19**, 298–308.
41 K. Kremer and G. S. Grest, *J. Chem. Phys.*, 1990, **92**, 5057–5086.
42 R. W. Hockney and J. W. Eastwood, *Computer Simulation Using Particles*, Adam Hilger, Bristol, 1988.
43 G. S. Grest and K. Kremer, *Phys. Rev. A: At., Mol., Opt. Phys.*, 1986, **33**, 3628–3631.
44 R. Konradi and J. Rühe, *Macromolecules*, 2005, **38**, 6140–6151.
45 E. M. Mateescu, C. Jeppesen and P. Pincus, *Europhys. Lett.*, 1999, **46**, 493–498.
46 A. G. Cherstvy and R. G. Winkler, *J. Phys. Chem. B*, 2005, **109**, 2962–2969.
47 O. Pyshkina, V. Sergeyev, A. Zezin, V. Kabanov, D. Gage and M. C. Stuart, *Langmuir*, 2003, **19**, 2000–2006.
48 A. Ishikubo, J. Mays and M. Tirrell, *Ind. Eng. Chem. Res.*, 2008, **47**, 6426–6433.
49 L. Samokhina, M. Schrinner and M. Ballauff, *Langmuir*, 2007, **23**, 3615–3619.
50 W. Zhuang, E. Kasëmi, Y. Ding, M. Kröger, A. D. Schlüter and J. P. Rabe, *Adv. Mater.*, 2008, **20**, 3204–3210.
51 Y. Y. Xu, O. V. Borisov, M. Ballauff and A. H. E. Müller, *Langmuir*, 2010, **26**, 6919–6926.
52 A. Halperin, M. Tirrell and T. Lodge, *Adv. Polym. Sci.*, 1992, **100**, 31–71.
53 S. V. Larin, D. V. Pergushov, Y. Y. Xu, A. A. Darinskii, A. B. Zezin, A. H. E. Müller and O. V. Borisov, *Soft Matter*, 2009, **5**, 4938–4943.

